Available online at www.sciencedirect.com
SCIENCE DIRECT®
Applied Numerical Mathematics 56 (2006) 589–607
APPLIED NUMERICAL MATHEMATICS
www.elsevier.com/locate/apnum

Optimally-stable second-order accurate difference schemes for non-linear conservation laws in 3D

Milan Kucharík [a], Richard Liska [a,*], Stanly Steinberg [b], Burton Wendroff [c]

[a] *Faculty of Nuclear Sciences and Physical Engineering, Czech Technical University in Prague, Břehová 7, 115 19 Prague 1, Czech Republic*
[b] *Department of Mathematics and Statistics, University of New Mexico, Albuquerque, NM 87131, USA*
[c] *Group T-7, Los Alamos National Laboratory, Los Alamos, NM 87544, USA*

Available online 13 May 2005

Abstract

In one and two spatial dimensions, Lax–Wendroff schemes provide second-order accurate optimally-stable dispersive conservation-form approximations to non-linear conservation laws. These approximations are an important ingredient in sophisticated simulation algorithms for conservation laws whose solutions are discontinuous. Straightforward generalization of these Lax–Wendroff schemes to three dimensions produces an approximation that is unconditionally unstable. However, some dimensionally-split schemes do provide second-order accurate optimally-stable approximations in 3D (and 2D), and there are sub-optimally-stable non-split Lax–Wendroff-type schemes in 3D. The main result of this paper is the creation of new Lax–Wendroff-type second-order accurate optimally-stable dispersive non-split scheme that is in conservation form. The scheme is created by using linear equivalence to transform a symmetrized dimensionally-split scheme (based on a one-dimensional Lax–Wendroff scheme) to conservation form. We then create both composite and hybrid schemes by combining the new scheme with the diffusive first-order accurate Lax–Friedrichs scheme. Codes based on these schemes perform well on difficult fluid flow problems.

Keywords: Conservation laws; Multidimensional finite difference schemes; Stability; Lax–Wendroff scheme

* Corresponding author.
E-mail addresses: kucharik@karkulka.fjfi.cvut.cz (M. Kucharík), liska@siduri.fjfi.cvut.cz (R. Liska), stanly@math.unm.edu (S. Steinberg), bbw@lanl.gov (B. Wendroff).
URLs: http://www-troja.fjfi.cvut.cz/~kucharik, http://www-troja.fjfi.cvut.cz/~liska, http://www.math.unm.edu/~stanly, http://www.math.unm.edu/~bbw.

0168-9274/$30.00 © 2005 IMACS. Published by Elsevier B.V. All rights reserved.
doi:10.1016/j.apnum.2005.04.004

1. Introduction

Three-dimensional systems of hyperbolic conservation laws have the form

$$U_t = f(U)_x + g(U)_y + h(U)_z, \tag{1}$$

where $U(t, x, y, z)$ is a vector of unknowns, f, g, h are smooth functions, and subscripts indicate partial derivatives. (Two-dimensional systems are obtained by assuming U is independent of z and 1D systems are obtained from 2D systems by assuming that U is independent of y.) Our goal is to find a second-order accurate optimally-stable, non-split discretization of (1) and then combine this discretization with a diffusive discretization to produce composite or hybrid schemes that will effectively solve problems with shock or contact discontinuities.

Stability is assessed by applying von-Neumann stability analysis to the discretization applied to the scalar linear conservation law (advection equation), that is, where U is a scalar function and $f(U) = a\,U$, $g(U) = b\,U$, and $h(U) = c\,U$, and where a, b, and c are constants. For a uniform space–time grid with spacing Δt, Δx, Δy and Δz, the stability region is given in terms of the dimensionless CFL numbers $\lambda = a\,\Delta x/\Delta t$, $\mu = b\,\Delta x/\Delta t$ and $\tau = c\,\Delta x/\Delta t$. It is well known that stability of an explicit scheme implies that $|\lambda| \leqslant 1$, $|\mu| \leqslant 1$ and $|\tau| \leqslant 1$. Optimally-stable schemes in 3D are those that have the this cube as their stability region (square in 2D and interval in 1D).

One of best known classical finite difference schemes for solving 1D conservation laws is the optimally-stable second-order accurate Lax–Wendroff (LW) scheme. In [11], a 2D optimally-stable second-order accurate variant of the LW scheme was created by approximately solving 1D Riemann problems on the edges of grid cells. Unfortunately, the generalization of this scheme to 3D is unconditionally unstable [11]. In [12], this unstable scheme was modified to produce two sub-optimally-stable schemes. Also, a family of 3D schemes with their stability and accuracy analysis has been presented in [8].

A common method of extending a 1D scheme to multiple dimensions is to use dimensional splitting (described below). However, the simplest dimensionally-split schemes are not symmetric, and even the well-known Strang splitting [16] is not symmetric, and these asymmetries produces noticeable adverse effects in simulations. Dimensional splitting can be symmetrized, but then the scheme becomes computationally costly. If two schemes are considered *linearly equivalent* if they reduce to the same scheme when f, g and h are linear (when the conservation law is linear), then equivalent schemes will have the same linear stability and accuracy, and we can hope that equivalent schemes will have similar non-linear properties. Here we create a Lax–Wendroff-type symmetric optimally-stable second-order accurate non-split scheme linearly equivalent to the fully-symmetric dimensionally-split LW scheme.

The modified equation for a scheme is found by expanding the scheme in a Taylor series in the time and spatial steps and then grouping the terms according to the degree of homogeneity in the steps. The zero-order term must be the original equation while the next non-zero term will contain derivatives of the solution of the original equation of some order. If this order is odd, then the scheme is called dispersive, otherwise it is diffusive or anti-diffusive. Generally, for stable schemes, first-order accurate schemes are diffusive, while second-order accurate schemes are dispersive. Because Lax–Wendroff schemes are always dispersive, they produce solutions that oscillate near discontinuities and, in particular, oscillate behind shocks. The schemes we use for practical computation of complex flows are made by combining a dispersive scheme with a diffusive, first-order accurate Lax–Friedrichs scheme to form either composite or hybrid schemes.

2. Lax–Friedrichs and Lax–Wendroff schemes

The simplest schemes for hyperbolic conservation laws are the first-order accurate diffusive Lax–Friedrichs schemes and the second-order accurate dispersive Lax–Wendroff schemes. We use schemes that can be written in predictor–corrector form in a staggered grid. The staggered grid consists of a primary grid where points are labeled with (i, j, k) and a dual grid where points are labeled with $(i + \frac{1}{2}, j + \frac{1}{2}, k + \frac{1}{2})$. In 3D, the centers of the cell faces of the primary grid are given by $(i + \frac{1}{2}, j + \frac{1}{2}, k)$, etc., while the center of cell edges in the primary grid are given by $(i + \frac{1}{2}, j, k)$, etc. In 2D, the centers of the cell edges in the primary grid are given by $(i + \frac{1}{2}, j)$, etc.

2.1. 1D schemes

The predictor for the 1D Lax–Friedrichs (LF) scheme computes values on the dual grid from values on the primary grid:

$$U_{i+1/2}^{n+1/2} = \frac{1}{2}\big(U_i^n + U_{i+1}^n\big) + \frac{\Delta t}{2\Delta x}\big(f\big(U_{i+1}^n\big) - f\big(U_i^n\big)\big), \tag{2}$$

while the corrector is defined by the same formula with both the i and n indices shifted by one-half and thus it computes values on the primary grid from values on the dual grid. This predictor–corrector scheme is less diffusive than the one-step variant, first-order accurate and optimally stable.

The Lax–Wendroff (LW) scheme uses the predictor (2) for the LF scheme and the corrector

$$U_i^{n+1} = U_i^n + \frac{\Delta t}{\Delta x}\big(f\big(U_{i+1/2}^{n+1/2}\big) - f\big(U_{i-1/2}^{n+1/2}\big)\big) \tag{3}$$

and is optimally stable, second-order accurate, dispersive, and in conservation from.

2.2. 2D schemes

In 2D, the predictor for the two-step forms of LF and LW schemes is [11]

$$\begin{aligned} U_{i+1/2,j+1/2}^{n+1/2} = {} & \frac{1}{4}\big(U_{i,j}^n + U_{i+1,j}^n + U_{i,j+1}^n + U_{i+1,j+1}^n\big) \\ & + \frac{\Delta t}{2\Delta x}\big(F_{i+1,j+1/2}^{n+1/4} - F_{i,j+1/2}^{n+1/4}\big) + \frac{\Delta t}{2\Delta x}\big(G_{i+1/2,j+1}^{n+1/4} - G_{i+1/2,j}^{n+1/4}\big), \end{aligned} \tag{4}$$

where the fluxes F and G are evaluated as the LF approximate solutions of the 1D Riemann problems at the center of edges of primary grid at time level $n + 1/4$:

$$\begin{aligned} F_{i,j+1/2}^{n+1/4} &= f\left(\frac{1}{2}\big(U_{i,j+1}^n + U_{i,j}^n\big) + \frac{\Delta t}{4\Delta x}\big(g\big(U_{i,j+1}^n\big) - g\big(U_{i,j}^n\big)\big)\right), \\ G_{i+1/2,j}^{n+1/4} &= g\left(\frac{1}{2}\big(U_{i+1,j}^n + U_{i,j}^n\big) + \frac{\Delta t}{\Delta y}4\big(f\big(U_{i+1,j}^n\big) - f\big(U_{i,j}^n\big)\big)\right). \end{aligned}$$

As in 1D, the LF corrector is the predictor with indices i, j, and n shifted by one half. The LW corrector uses central differencing in space and time:

$$U_{i,j}^{n+1} = U_{i,j}^{n} + \frac{\Delta t}{2\Delta x}\big(f\big(U_{i+1/2,j+1/2}^{n+1/2}\big) + f\big(U_{i+1/2,j-1/2}^{n+1/2}\big) - f\big(U_{i-1/2,j+1/2}^{n+1/2}\big) - f\big(U_{i-1/2,j-1/2}^{n+1/2}\big)\big)$$
$$+ \frac{\Delta t}{2\Delta y}\big(g\big(U_{i+1/2,j+1/2}^{n+1/2}\big) + g\big(U_{i-1/2,j+1/2}^{n+1/2}\big) - g\big(U_{i+1/2,j-1/2}^{n+1/2}\big) - g\big(U_{i-1/2,j-1/2}^{n+1/2}\big)\big).$$

The properties of these schemes are the same as in 1D.

2.3. 3D schemes

The straightforward generalization [12,11] of the 2D two-step LF and LW schemes lead to the predictor

$$\begin{aligned} U_{i+1/2,j+1/2,k+1/2}^{n+1/2} = {} & \frac{1}{8}\big(U_{i,j,k}^{n} + U_{i+1,j,k}^{n} + U_{i,j+1,k}^{n} + U_{i,j,k+1}^{n} \\ & + U_{i,j+1,k+1}^{n} + U_{i+1,j,k+1}^{n} + U_{i+1,j+1,k}^{n} + U_{i+1,j+1,k+1}^{n}\big) \\ & + \frac{\Delta t}{2\Delta x}\big(f\big(U_{i+1,j+1/2,k+1/2}^{n+1/4}\big) - f\big(U_{i,j+1/2,k+1/2}^{n+1/4}\big)\big) \\ & + \frac{\Delta t}{2\Delta y}\big(g\big(U_{i+1/2,j+1,k+1/2}^{n+1/4}\big) - g\big(U_{i+1/2,j,k+1/2}^{n+1/4}\big)\big) \\ & + \frac{\Delta t}{2\Delta z}\big(h\big(U_{i+1/2,j+1/2,k+1}^{n+1/4}\big) - h\big(U_{i+1/2,j+1/2,k}^{n+1/4}\big)\big). \end{aligned}$$

The values at the center of all faces of the primary cell on time level $n + 1/4$ are computed using the analog of 2D predictor (4):

$$\begin{aligned} U_{i,j+1/2,k+1/2}^{n+1/4} = {} & \frac{1}{4}\big(U_{i,j,k}^{n} + U_{i,j+1,k}^{n} + U_{i,j,k+1}^{n} + U_{i,j+1,k+1}^{n}\big) \\ & + \frac{\Delta t}{4\Delta y}\big(g\big(U_{i,j+1,k+1/2}^{n+1/6}\big) - g\big(U_{i,j,k+1/2}^{n+1/6}\big)\big) \\ & + \frac{\Delta t}{4\Delta z}\big(h\big(U_{i,j+1/2,k+1}^{n+1/6}\big) - h\big(U_{i,j+1/2,k}^{n+1/6}\big)\big), \end{aligned} \tag{5}$$

with similar formulas for the other faces. The values at the center of the edges of the primary cell on time level $n + 1/6$ are evaluated by an analog of 1D predictor (2):

$$U_{i+1/2,j,k}^{n+1/6} = \frac{1}{2}\big(U_{i,j,k}^{n} + U_{i+1,j,k}^{n}\big) + \frac{\Delta t}{6\Delta x}\big(f\big(U_{i+1,j,k}^{n}\big) - f\big(U_{i,j,k}^{n}\big)\big), \tag{6}$$

with similar formulas for the other edges. Again, as in 1D and 2D, the LF corrector involves the same formulas with the indices i, j, k and n shifted by a one half and produces optimally stable scheme, while the LW corrector uses:

$$U_{i,j,k}^{n+1} = U_{i,j,k}^{n} + \frac{\Delta t}{\Delta x}\big(F_{i+1/2,j,k} - F_{i-1/2,j,k}\big) + \frac{\Delta t}{\Delta y}\big(G_{i,j+1/2,k} - G_{i,j-1/2,k}\big)$$
$$+ \frac{\Delta t}{\Delta z}\big(H_{i,j,k+1/2} - H_{i,j,k-1/2}\big),$$

where the fluxes at the centers of the edges are given by simple averaging:

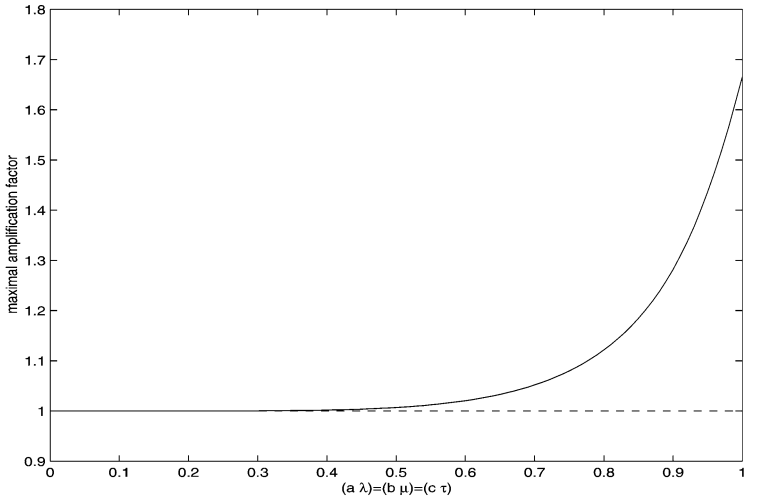

Fig. 1. The dependence of the maximum absolute value of the amplification factor over all three Fourier angles on the CFL number when $\lambda = \mu = \tau$ for the LW scheme in 3D.

$$F_{i+1/2,j,k} = \frac{1}{4}\big(f\big(U^{n+1/2}_{i+1/2,j+1/2,k+1/2}\big) + f\big(U^{n+1/2}_{i+1/2,j-1/2,k+1/2}\big) + f\big(U^{n+1/2}_{i+1/2,j+1/2,k-1/2}\big) + f\big(U^{n+1/2}_{i+1/2,j-1/2,k-1/2}\big)\big),$$

with similar formulas for the other edges.

Von Neumann stability analysis was used in [11] to prove that this two-step 3D LW scheme is unconditionally unstable (for the advection equation). Fig. 1 shows the dependence of maximum (over all three Fourier angles) of the absolute value of amplification factor on the CFL numbers when $\lambda = \mu = \tau$. For small CFL numbers the maximum amplification factor is very close to one and so the instability is very mild, e.g. for the CFL number $\lambda = \mu = \tau = 0.2$ the amplification factor has the value 1.00003 and the Fourier components of the solution will doubled only after more than 20 000 time steps because $1.00003^{20\,000} < 2$. Note that also in [8] some 3D discretizations are unconditionally unstable.

A possible way to stabilize this unstable scheme [12] is to use only an average when approximating values at the center of edges (6) (which is the same as using $C = 0$ in (7) given below). We have tried to generalize this idea further by introducing a time level $n + C$ (where $C \in [0, 1/4)$) instead of time level $n + \frac{1}{6}$ and replacing the values at the center of edges (6) by

$$U^{n+C}_{i+1/2,j,k} = \frac{1}{2}\big(U^{n}_{i,j,k} + U^{n}_{i+1,j,k}\big) + C\frac{\Delta t}{\Delta x}\big(f\big(U^{n}_{i+1,j,k}\big) - f\big(U^{n}_{i,j,k}\big)\big). \tag{7}$$

This gives a family of difference schemes depending on the parameter C. Stability regions of these schemes have been estimated by numerical sampling of the amplification factor of the schemes. The largest stability region was obtained when $C = 0$, for which the stability region includes the cube $\max(|\lambda|, |\mu|, |\tau|) < 0.854$. We call the scheme with $C = 0$ the corrected Friedrichs (CF) scheme.

We have also tried to use values at the center of cube faces (5) on a time level $n + D$ instead of $n + 1/4$, so introducing second parameter D. However varying both parameters did not lead to bigger stability region. Simpler 3D schemes with numerical fluxes at the center of faces being only averages of fluxes at corresponding four corners have been proposed in [12]. These schemes are computationally

fast, so we call them the fast LF (FLF) and the fast CF (FCF) schemes. Their disadvantage is that their stability region is given by the cube $\max(|\lambda|, |\mu|, |\tau|) < 1/\sqrt{3}$ which is rather small.

3. Optimally-stable schemes based on dimensional splitting

We will create optimally-stable schemes by starting with a simple dimensionally-split scheme, symmetrizing this scheme, and then transforming the result using linear equivalence to a nice non-split conservation form. In 3D, dimensionally-split schemes for the conservation laws (1) are created by successively approximating the solutions of the three 1D conservation laws $U_t = f(U)_x$, $U_t = g(U)_y$, and $U_t = h(U)_z$. The operators of the 1D solvers are called L_x, L_y and L_z. The symmetrized dimensionally-split scheme is given by averaging all possible simple dimensionally-split schemes. We then build a non-split scheme linearly equivalent to the symmetrized scheme by applying the transformations of type

$$\frac{1}{2}\big(f(A) + f(B)\big) \to f\left(\frac{A+B}{2}\right) \tag{8}$$

to all of the numerical fluxes given by f, g and h. Because linear equivalent schemes are the same for linear equations, they all have the same linear stability region and the same accuracy for linear equations. When A is a complicated expression and B is simple, we will write $B = f(A)$ as $f^{-1}(B) = A$ to simplify the formulas. After the derivation, we explicitly show that the scheme is second-order accurate also for non-linear problems.

In 2D we do have an optimally-stable second-order LW-type difference scheme CF. However we first present the derivation of a different non-split optimally-stable second-order scheme from dimensionally split one in 2D as the procedure is much simpler and easier to understand in 2D than in 3D. Then we will use the same method to derive new 3D scheme.

3.1. 2D split schemes

A simple non-symmetric dimensionally-split scheme (NSS) is

$$U_{i,j}^{n+1} = L^y L^x U_{i,j}^n.$$

The 1D numerical solution operators L^x and L^y are given by the 1D LW scheme (2)–(3) rewritten to 2D:

$$\begin{aligned}
L^x\big(U_{i,j}^n\big) &= U_{i,j}^n + \frac{\Delta t}{\Delta x}\big(f\big(U_{i+1/2,j}^{n+1/2}\big) - f\big(U_{i-1/2,j}^{n+1/2}\big)\big)\\
L^y\big(U_{i,j}^n\big) &= U_{i,j}^n + \frac{\Delta t}{\Delta y}\big(g\big(U_{i,j+1/2}^{n+1/2}\big) - g\big(U_{i,j-1/2}^{n+1/2}\big)\big)\\
U_{i+1/2,j}^{n+1/2} &= \frac{1}{2}\big(U_{i,j}^n + U_{i+1,j}^n\big) + \frac{\Delta t}{2\Delta x}\big(f\big(U_{i+1,j}^n\big) - f\big(U_{i,j}^n\big)\big)\\
U_{i,j+1/2}^{n+1/2} &= \frac{1}{2}\big(U_{i,j}^n + U_{i,j+1}^n\big) + \frac{\Delta t}{2\Delta y}\big(g\big(U_{i,j+1}^n\big) - g\big(U_{i,j}^n\big)\big).
\end{aligned} \tag{9}$$

This scheme is theoretically only first-order accurate and optimally stable. Note that the Strang splitting $L^x L^y L^y L^x$ [16] is second-order but not symmetric.

The symmetrized dimensionally-split scheme (SYS) is

$$U_{i,j}^{n+1} = \frac{1}{2}\big(L^x L^y + L^y L^x\big)\big(U_{i,j}^n\big). \tag{10}$$

Clearly SYS is computationally twice as costly as NSS, but it is second-order accurate, symmetric and optimally stable.

3.2. 2D non-split schemes

We now transform the split scheme SYS (10) to a non-split scheme using linear equivalence (8). The first part of the combined operator (10) is

$$\begin{aligned}\big(L^x L^y\big)\big(U_{i,j}^n\big) &= L^y\big(U_{i,j}^n\big) + \frac{\Delta t}{\Delta x}\big(f\big(L^y U\big)_{i+1/2,j}^{n+1/2} - f\big(L^y U\big)_{i-1/2,j}^{n+1/2}\big)\\ &= U_{i,j}^n + \frac{\Delta t}{\Delta y}\big(g\big(U_{i,j+1/2}^{n+1/2}\big) - g\big(U_{i,j-1/2}^{n+1/2}\big)\big) + \frac{\Delta t}{\Delta x}\big(f\big(L^y U\big)_{i+1/2,j}^{n+1/2} - f\big(L^y U\big)_{i-1/2,j}^{n+1/2}\big)\end{aligned}$$

with an analogous expression for the second part. Linear equivalence can be used to transform SYS into conservation form:

$$\begin{aligned}U_{i,j}^{n+1} &= \frac{1}{2}\big(L^x L^y + L^y L^x\big)\big(U_{i,j}^n\big)\\ &= U_{i,j}^n + \frac{\Delta t}{\Delta x}\big(F_{i+1/2,j}^{n+1/2} - F_{i-1/2,j}^{n+1/2}\big) + \frac{\Delta t}{\Delta y}\big(G_{i,j+1/2}^{n+1/2} - G_{i,j-1/2}^{n+1/2}\big),\end{aligned} \tag{11}$$

where

$$F_{i+1/2,j}^{n+1/2} = f\bigg(\frac{1}{2}\big(U_{i+1/2,j}^{n+1/2} + \big(L^y U\big)_{i+1/2,j}^{n+1/2}\big)\bigg).$$

The first term in the argument of f results from the $L^y L^x U$ part of (10) and the second one from the $L^x L^y U$ part. Now we substitute for $U_{i+1/2,j}^{n+1/2}$ using (9) and for $(L^y U)_{i+1/2,j}^{n+1/2}$ using the same formula, just replacing U by $L^y U$, to obtain

$$\begin{aligned}f^{-1}\big(F_{i+1/2,j}^{n+1/2}\big) &= \frac{1}{4}\big(U_{i,j}^n + U_{i+1,j}^n\big) + \frac{\Delta t}{4\Delta x}\big(f\big(U_{i+1,j}^n\big) - f\big(U_{i,j}^n\big)\big)\\ &\quad + \frac{1}{4}\big(\big(L^y U\big)_{i,j}^n + \big(L^y U\big)_{i+1,j}^n\big) + \frac{\Delta t}{4\Delta x}\big(f\big(L^y U\big)_{i+1,j}^n - f\big(L^y U\big)_{i,j}^n\big).\end{aligned}$$

After substitution for $L^y U$ from (9) and another linear-equivalence transformation of the fluxes, we obtain the final formula for numerical flux:

$$\begin{aligned}f^{-1}\big(F_{i+1/2,j}^{n+1/2}\big) &= \frac{1}{2}\big(U_{i,j}^n + U_{i+1,j}^n\big) + \frac{\Delta t}{4\Delta y}\big(g_{i,j+1/2}^{n+1/2} + g_{i+1,j+1/2}^{n+1/2} - g_{i,j-1/2}^{n+1/2} - g_{i+1,j-1/2}^{n+1/2}\big)\\ &\quad + \frac{\Delta t}{2\Delta x}\bigg(f\bigg(U_{i+1,j}^n + \frac{\Delta t}{2\Delta y}\big(g_{i+1,j+1/2}^{n+1/2} - g_{i+1,j-1/2}^{n+1/2}\big)\bigg)\\ &\quad - f\bigg(U_{i,j}^n + \frac{\Delta t}{2\Delta y}\big(g_{i,j+1/2}^{n+1/2} - g_{i,j-1/2}^{n+1/2}\big)\bigg)\bigg),\end{aligned}$$

where the symbols g with indices means the flux function evaluated at the value of U with the same indices. Values on the time level $n + \frac{1}{2}$ are computed from (9). The 2D dimensional splitting based scheme (DSBS) is obtained by repeating this process for G.

3.3. 2D stability and accuracy

Because DSBS is linearly equivalent to SYS, and SYS is optimally stable, then so is DSBS. However we will independently check this result. The amplification factor of DSBS for the special case $\mu = \lambda$ is

$$\left|g(\alpha,\beta)\right|^2 = 1 - 4\frac{\lambda^2(1-\lambda^2)}{(1+t_a^2)^2(1+t_b^2)^2}T,$$

where

$$T = 4\lambda^4 t_a^4 t_b^4 - 4\lambda^2 t_a^4 t_b^4 + 2t_a^4 t_b^4 + 2t_a^4 t_b^2 + 2t_a^2 t_b^4 + t_a^4 + t_b^4,$$

where $t_a = \tan(\alpha/2)$, $t_b = \tan(\beta/2)$, and α and β are the Fourier angles. Using a computer algebra program for quantifier elimination [4,1], we proved that $|g(\alpha,\beta)|^2 \leqslant 1$ for all α and β if and only if $|\lambda| \leqslant 1$, so the scheme is optimally stable in this case. Using the same approach for the general case $\lambda \neq \mu$, we proved that DSBS is optimally stable.

Because of the linear equivalence, the scheme will be second-order accurate for the linear advection equation. For non-linear fluxes, the situation is not obvious as the transformations during the construction might disturb the accuracy. However, DSBS is symmetric in the spatial indices, so we expect it to be second-order in the spatial variables. A Taylor expansion of the scheme in Δt, Δx and Δy gives

$$U_t - f'U_x - g'U_y + \frac{1}{2}\Delta t T + \mathrm{O}\left(\Delta t^2\right) = 0, \tag{12}$$

where

$$T = U_{tt} - f'^2 U_{xx} - g'^2 U_{yy} - 2f'f''U_x^2 - 2g'g''U_y^2 - 2U_xU_y(f'g'' + f''g') - 2f'g'U_{xy}.$$

If we differentiate (12) with respect to t and keep only zeroth order terms in Δt we get

$$U_{tt} - f''U_tU_x - f'U_{tx} - g''U_tU_y - g'U_{ty} = 0,$$

which, after elimination of U_t, U_{tx} and U_{ty} by using (12) and its space derivatives, transforms into $T = 0$ and thus DSBS is second-order accurate for general fluxes.

So DSBS is second-order accurate, non-split, symmetric and optimally stable.

3.4. 3D split schemes

The simple 3D non-symmetric dimensionally-split scheme (3D NSS) is given by

$$U_{i,j,k}^{n+1} = L^x L^y L^z U_{i,j,k}^n,$$

where the operators L^x and L^y are defined by (9) and the operator L^z is defined analogously. This scheme is simple, fast, non-symmetric and optimally stable. Theoretically it is only first-order accurate, however practically it is second-order as seen in Table 2 below.

In 3D there are 6 different products of the operators L^x, L^y, and L^z, so to make a symmetrized dimensionally-split scheme (SYS), we average these combinations:

$$U_{i,j,k}^{n+1} = \frac{1}{6}\left(L^xL^yL^z + L^xL^zL^y + L^yL^xL^z + L^yL^zL^x + L^zL^xL^y + L^zL^yL^x\right)\left(U_{i,j,k}^n\right). \tag{13}$$

This scheme is second-order accurate, symmetric and optimally stable.

3.5. 3D non-split schemes

As in 2D, we will start with one term in 3D SYS (13) and transform it using linear equivalence (8):

$$\begin{aligned}\left(L^z L^x L^y\right)\left(U^n_{i,j,k}\right) &= \left(L^x L^y\right)\left(U^n_{i,j,k}\right) + \frac{\Delta t}{\Delta z}\left(h\left(L^x L^y U\right)^{n+1/2}_{i,j,k+1/2} - h\left(L^x L^y U\right)^{n+1/2}_{i,j,k-1/2}\right)\\ &= U^n_{i,j,k} + \frac{\Delta t}{\Delta y}\left(g\left(U^{n+1/2}_{i,j+1/2}\right) - g\left(U^{n+1/2}_{i,j-1/2}\right)\right)\\ &\quad + \frac{\Delta t}{\Delta x}\left(f\left(L^y U\right)^{n+1/2}_{i+1/2,j,k} - f\left(L^y U\right)^{n+1/2}_{i-1/2,j,k}\right)\\ &\quad + \frac{\Delta t}{\Delta z}\left(h\left(L^x L^y U\right)^{n+1/2}_{i,j,k+1/2} - h\left(L^x L^y U\right)^{n+1/2}_{i,j,k-1/2}\right).\end{aligned}$$

The other terms can be transformed in the same way. To get the conservation form

$$\begin{aligned}U^{n+1}_{i,j,k} = U^n_{i,j,k} &+ \frac{\Delta t}{\Delta x}\left(F^{n+1/2}_{i+1/2,j,k} - F^{n+1/2}_{i-1/2,j,k}\right) + \frac{\Delta t}{\Delta y}\left(G^{n+1/2}_{i,j+1/2,k} - G^{n+1/2}_{i,j-1/2,k}\right)\\ &+ \frac{\Delta t}{\Delta z}\left(H^{n+1/2}_{i,j,k+1/2} - H^{n+1/2}_{i,j,k-1/2}\right)\end{aligned} \tag{14}$$

of 3D SYS (13), we use linear equivalence to collect all terms with same flux at same point, e.g. for the point $(n+\frac{1}{2}, i+\frac{1}{2}, j, k)$ we get $F^{n+1/2}_{i+1/2,j,k}$

$$\begin{aligned}F^{n+1/2}_{i+1/2,j,k} = f\Bigg(&\frac{1}{3}U^{n+1/2}_{i+1/2,j,k} + \frac{1}{6}\left(\left(L^y U\right)^{n+1/2}_{i+1/2,j,k} + \left(L^z U\right)^{n+1/2}_{i+1/2,j,k}\right)\\ &+ \frac{1}{6}\left(\left(L^y L^z U\right)^{n+1/2}_{i+1/2,j,k} + \left(L^z L^y U\right)^{n+1/2}_{i+1/2,j,k}\right)\Bigg).\end{aligned}$$

Next we move first from staggered grid (in index i) to original grid and then expand the outer operator in terms $L^y L^z$ and $L^z L^y$, and then move from staggered grid again, and finally expand all remaining operators L^y and L^z to get the final numerical flux:

$$\begin{aligned}f^{-1}\left(F^{n+1/2}_{i+1/2,j,k}\right) = &\frac{1}{2}\left(U^n_{i+1,j,k} + U^n_{i,j,k}\right) + \frac{\Delta t}{6\Delta z}\left(h^{n+1/2}_{i+1,j,k+1/2} - h^{n+1/2}_{i+1,j,k-1/2}\right)\\ &+ \frac{\Delta t}{6\Delta z}\left(h^{n+1/2}_{i,j,k+1/2} - h^{n+1/2}_{i,j,k-1/2}\right) + \frac{\Delta t}{6\Delta y}\left(g^{n+1/2}_{i+1,j+1/2,k} - g^{n+1/2}_{i+1,j-1/2,k}\right)\\ &+ \frac{\Delta t}{6\Delta y}\left(g^{n+1/2}_{i,j+1/2,k} - g^{n+1/2}_{i,j-1/2,k}\right) + \frac{\Delta t}{12\Delta z}\left(\widehat{H}^{n+1/2}_{i+1,j,k+1/2} - \widehat{H}^{n+1/2}_{i+1,j,k-1/2}\right)\\ &+ \frac{\Delta t}{12\Delta z}\left(\widehat{H}^{n+1/2}_{i,j,k+1/2} - \widehat{H}^{n+1/2}_{i,j,k-1/2}\right) + \frac{\Delta t}{12\Delta y}\left(\widehat{G}^{n+1/2}_{i+1,j+1/2,k} - \widehat{G}^{n+1/2}_{i+1,j-1/2,k}\right)\\ &+ \frac{\Delta t}{12\Delta y}\left(\widehat{G}^{n+1/2}_{i,j+1/2,k} - \widehat{G}^{n+1/2}_{i,j-1/2,k}\right)\\ &+ \frac{\Delta t}{2\Delta x}\Bigg(f\Bigg[U^n_{i+1,j,k} + \frac{\Delta t}{3\Delta y}\left(g^{n+1/2}_{i+1,j+1/2,k} - g^{n+1/2}_{i+1,j-1/2,k}\right)\\ &+ \frac{\Delta t}{3\Delta z}\left(h^{n+1/2}_{i+1,j,k+1/2} - h^{n+1/2}_{i+1,j,k-1/2}\right) + \frac{\Delta t}{6\Delta z}\left(\widehat{H}^{n+1/2}_{i+1,j,k+1/2} - \widehat{H}^{n+1/2}_{i+1,j,k-1/2}\right)\end{aligned}$$

$$+\frac{\Delta t}{6\Delta y}\big(\widehat{G}^{n+1/2}_{i+1,j+1/2,k}-\widehat{G}^{n+1/2}_{i+1,j-1/2},k\big)\Bigg]$$
$$-f\Bigg[U^n_{i,j,k}+\frac{\Delta t}{3\Delta y}\big(g^{n+1/2}_{i,j+1/2,k}-g^{n+1/2}_{i,j-1/2,k}\big)+\frac{\Delta t}{3\Delta z}\big(h^{n+1/2}_{i,j,k+1/2}-h^{n+1/2}_{i,j,k-1/2}\big)$$
$$+\frac{\Delta t}{6\Delta z}\big(\widehat{H}^{n+1/2}_{i,j,k+1/2}-\widehat{H}^{n+1/2}_{i,j,k-1/2}\big)+\frac{\Delta t}{6\Delta y}\big(\widehat{G}^{n+1/2}_{i,j+1/2,k}-\widehat{G}^{n+1/2}_{i,j-1/2,k}\big)\Bigg]\Bigg), \tag{15}$$

where

$$\widehat{H}^{n+1/2}_{i,j,k+1/2}=h\Bigg(\frac{1}{2}\big(U^n_{i,j,k+1}+U^n_{i,j,k}\big)+\frac{\Delta t}{2\Delta y}\big(g^{n+1/2}_{i,j+1/2,k+1}-g^{n+1/2}_{i,j-1/2,k+1}\big)$$
$$+\frac{\Delta t}{2\Delta y}\big(g^{n+1/2}_{i,j+1/2,k}-g^{n+1/2}_{i,j-1/2,k}\big)$$
$$+\frac{\Delta t}{2\Delta z}\Bigg[h\Bigg(U^n_{i,j,k+1}+\frac{\Delta t}{\Delta y}\big(g^{n+1/2}_{i,j+1/2,k+1}-g^{n+1/2}_{i,j-1/2,k+1}\big)\Bigg)$$
$$-h\Bigg(U^n_{i,j,k}+\frac{\Delta t}{\Delta y}\big(g^{n+1/2}_{i,j+1/2,k}-g^{n+1/2}_{i,j-1/2,k}\big)\Bigg)\Bigg]\Bigg). \tag{16}$$

Similarly

$$\widehat{G}^{n+1/2}_{i,j+1/2,k}=g\Bigg(\frac{1}{2}\big(U^n_{i,j+1,k}+u^n_{i,j,k}\big)+\frac{\Delta t}{2\Delta z}\big(h^{n+1/2}_{i,j+1,k+1/2}-h^{n+1/2}_{i,j+1,k-1/2}\big)$$
$$+\frac{\Delta t}{2\Delta z}\big(h^{n+1/2}_{i,j,k+1/2}-h^{n+1/2}_{i,j,k-1/2}\big)$$
$$+\frac{\Delta t}{2\Delta y}\Bigg[g\Bigg(U^n_{i+1,j,k}+\frac{\Delta t}{2\Delta z}\big(h^{n+1/2}_{i,j+1,k+1/2}-h^{n+1/2}_{i,j+1,k-1/2}\big)\Bigg)$$
$$-g\Bigg(U^n_{i,j,k}+\frac{\Delta t}{2\Delta z}\big(h^{n+1/2}_{i,j,k+1/2}-h^{n+1/2}_{i,j,k-1/2}\big)\Bigg)\Bigg]\Bigg). \tag{17}$$

Similar expressions for the other numerical fluxes $G^{n+1/2}_{i,j+1/2,k}$ and $H^{n+1/2}_{i,j,k+1/2}$ can be derived using the same process. The 3D dimensional splitting based scheme (3D DSBS) is then defined by (14).

3.6. 3D stability and accuracy

Because 3D DSBS is linearly equivalent to 3D SYS, it has to be optimally stable and second-order accurate for the advection equation. For general non-linear fluxes, the Taylor expansion of the 3D DSBS gives

$$U_t-f'U_x-g'U_y-h'U_z+\frac{\Delta t}{2}T+\mathrm{O}\big(\Delta t^2\big)=0, \tag{18}$$

where

$$T=U_{tt}-2f'f''U_x^2-2g'g''U_y^2-2h'h''U_z^2-f'^2U_{xx}-g'^2U_{yy}-h'^2U_{zz}-2f'g'U_{xy}-2f'h'U_{xz}$$
$$-2g'h'U_{yz}-2U_xU_y(f'g''+f''g')-2U_xU_z(f'h''+f''h')-2U_yU_z(g'h''+g''h'). \tag{19}$$

As in 2D, the elimination of U_{tt} and other time derivatives by differentiation of (18) and subsequent substitutions results in $T = 0$, and thus 3D DSBS is second-order accurate for general fluxes. So DSBS is second-order accurate, non-split, optimally stable, symmetric scheme.

4. Practical schemes

Solutions of non-linear conservation laws commonly contain shocks or contact waves and thus are discontinuous. Simple dispersive schemes will display oscillations near the discontinuities, while diffusive schemes will smooth the discontinuities excessively. It is common practice to combine dispersive and diffusive schemes to obtain practical schemes for producing quality solutions of non-linear conservation laws. We have implemented two types of schemes: composite [12] and hybrid [3] schemes.

4.1. Composite schemes

Composite schemes [12] add diffusivity to a dispersive scheme by taking a time step with the diffusive scheme every few steps taken with the dispersive scheme. In contrast with the hybrid methods described next, this adds diffusivity globally, not just near the discontinuities, the advantage being that composite schemes are less costly. When we combine optimally-stable dispersive second-order-accurate scheme with an optimally-stable diffusive first-order scheme, we obtain an optimally-stable first-order scheme. The scheme that combines $n-1$ steps of the LW scheme followed by one step of the LF scheme is labeled LW LF n, with typically $n = 4$. In 3D we use CF, FCF or DSBS instead of LW to obtain optimally-stable CF LF n, FCF LF n and DSBS LF n schemes.

4.2. Hybrid schemes

Hybrid schemes add diffusivity locally by combining a dispersive flux with a diffusive flux with a switch that only applies the diffusion near the discontinuities. For example, for LW and LF,

$$U_i^{n+1} = U_i^n + (F_{i+1/2} - F_{i-1/2}),$$

where

$$F_{i+1/2} = \alpha_{i+1/2} F_{i+1/2}^{\mathrm{LF}} + (1 - \alpha_{i+1/2}) F_{i+1/2}^{\mathrm{LW}}.$$

The switch $\alpha_{i+1/2} \in [0, 1]$ should be zero in smooth regions and one near discontinuities so that the hybrid scheme keeps second-order accuracy in smooth regions, is first-order near discontinuities, but removes any oscillation near the discontinuity. In 1D and 2D, we use LW as the dispersive scheme, while in 3D we use CF, FCF or DSBS for the dispersive scheme.

We have tested several switches from [7] and found that the Harten switch [2] had the best behavior:

$$\alpha_{i+1/2} = \max\bigl(\Theta_i^n, \Theta_{i+1}^n\bigr),$$

where

$$\Theta_i^n = \begin{cases} \kappa \left| \dfrac{|U_{i+1}^n - U_i^n| - |U_i^n - U_{i-1}^n|}{|U_{i+1}^n - U_i^n| + |U_i^n - U_{i-1}^n|} \right|^m & \text{for } |U_{i+1}^n - U_i^n| + |U_i^n - U_{i-1}^n| > \delta \\ 0 & \text{for } |U_{i+1}^n - U_i^n| + |U_i^n - U_{i-1}^n| \leqslant \delta. \end{cases}$$

Here $\delta > 0$ is a parameter which avoids division by a small numbers, $0 \leqslant \kappa \leqslant 1$ and $m \geqslant 1$. In multiple dimensions, we apply the switch each direction independently. The extra cost of the hybrid scheme is that we must compute both fluxes and the switch in each time step and all spatial points. The advantage is that hybrids schemes remain second-order in regions where the solution is smooth.

For the hybrid scheme we need to put the 3D LF scheme into conservation form:

$$U_{i,j,k}^{n+1} = U_{i,j,k}^{n} + \big(\widehat{F}_{i+1/2,j,k}^{n+1/2} - \widehat{F}_{i-1/2,j,k}^{n+1/2}\big) + \big(\widehat{G}_{i,j+1/2,k}^{n+1/2} - \widehat{G}_{i,j-1/2,k}^{n+1/2}\big) + \big(\widehat{H}_{i,j,k+1/2}^{n+1/2} - \widehat{H}_{i,j,k-1/2}^{n+1/2}\big).$$

The most complicated part of deriving the LF numerical fluxes is the splitting of averages on different levels and collecting them into the numerical fluxes. The final expression for the numerical flux is

$$\begin{aligned}
\widehat{F}_{i+1/2,j,k}^{n+1/2} = {} & \frac{1}{2}\frac{\Delta t}{\Delta x} f\big(U_{i+1/2,j,k}^{n+3/4}\big) + \frac{\Delta t}{16\Delta x}\big(f\big(U_{i+1,j+1/2,k+1/2}^{n+1/4}\big) + f\big(U_{i,j+1/2,k+1/2}^{n+1/4}\big)\big) \\
& + \frac{\Delta t}{16\Delta x}\big(f\big(U_{i+1,j+1/2,k-1/2}^{n+1/4}\big) + f\big(U_{i,j+1/2,k-1/2}^{n+1/4}\big)\big) \\
& + \frac{\Delta t}{16\Delta x}\big(f\big(U_{i+1,j-1/2,k+1/2}^{n+1/4}\big) + f\big(U_{i,j-1/2,k+1/2}^{n+1/4}\big)\big) \\
& + \frac{\Delta t}{16\Delta x}\big(f\big(U_{i+1,j-1/2,k-1/2}^{n+1/4}\big) + f\big(U_{i,j-1/2,k-1/2}^{n+1/4}\big)\big) \\
& + \frac{1}{192}\sum_{\pm}\big(U_{i+1,j\pm1,k\pm1}^{n} - U_{i,j\pm1,k\pm1}^{n}\big) + \frac{1}{48}\sum_{\pm}\big(U_{i+1,j\pm1,k}^{n} - U_{i,j\pm1,k}^{n}\big) \\
& + \frac{1}{48}\sum_{\pm}\big(U_{i+1,j,k\pm1}^{n} - U_{i,j,k\pm1}^{n}\big) + \frac{7}{48}\big(U_{i+1,j,k}^{n} - U_{i,j,k}^{n}\big),
\end{aligned}$$

where the values for $U^{n+3/4}$, $U^{n+4/6}$, $U^{n+1/2}$, $U^{n+1/4}$ and $U^{n+1/6}$ are obtained from the appropriate equations (5) and (6) for the standard 3D LF scheme. The other numerical fluxes $\widehat{G}$, $\widehat{H}$ are derived analogously.

We have implemented all of the described schemes in all dimensions [6]:

- CF—Corrected Friedrichs, non-split, not optimally stable.
- FCF—Fast Corrected Friedrichs, non-split, not optimally stable.
- NSS—Non-Symmetric Split, split, optimally stable.
- SYS—Symmetric Split, split, optimally stable.
- DSBS—Dimensional Splitting Based Scheme, non-split, optimally stable.

In the next section we will report on numerical tests of the 3D implementations of a modest selection of these schemes.

5. Numerical tests

To test our schemes, we use the 3D Euler equations [10]:

$$\begin{pmatrix} \rho \\ \rho u \\ \rho v \\ \rho w \\ E \end{pmatrix}_t + \begin{pmatrix} \rho u \\ \rho u^2 + p \\ \rho uv \\ \rho uw \\ u(E+p) \end{pmatrix}_x + \begin{pmatrix} \rho v \\ \rho uv \\ \rho v^2 + p \\ \rho vw \\ v(E+p) \end{pmatrix}_y + \begin{pmatrix} \rho w \\ \rho uw \\ \rho vw \\ \rho w^2 + p \\ w(E+p) \end{pmatrix}_z = 0,$$

where u, v and w are the components of the fluid velocity, ρ is the fluid density, p fluid pressure and E the density total energy density. The pressure and the energy are related by the equation of state of ideal gas,

$$E = \frac{p}{\gamma - 1} + \frac{1}{2}\rho\left(u^2 + v^2 + w^2\right),$$

where γ is the adiabatic gas index.

5.1. Implementation

For 3D problems, both the computational and storage cost can easily overwhelm a modern computer, so it is important to obtain a good balance between these costs. We can estimate the cost of storing the five dependent variables on a grid with N^3 cells as $5 \times 8 \times N^3$ bytes (one double float number requires 8 bytes). So for a grid with 300^3 points, this exceeds 1 GB. So we minimized the number of 3D arrays to one and substantially reduced the computation time by using a system of 2D arrays to store intermediate results. This causes interdependencies in the code, slowing the code a bit, but its benefits outweigh its disadvantages.

The time step is adaptively computed after each computational step as the minimum of the time steps over all grid cells with given CFL number and with wave speeds being the eigenvalues of Jacobian matrices in all three directions.

5.2. Numerical examples

Here we present numerical results for several problems:

- Smooth solution—We used this for comparing computing times and testing the basic properties of all elementary schemes.
- Noh problem—This is a difficult and practical problem with a shock and an analytic solution. We provide comparative tests for all five composite schemes.
- Explosion problem—The solution contains shock, contact, and rarefaction waves. Also, there is a Raleigh–Taylor instability that disappears if the scheme has too much diffusion, so we use very little diffusion.
- Riemann problem—The initial data for this problem starts with eight different values on eight octants that meet at a point, resulting in a solution with complex behavior. We use DSBSLF4 to provide a high-quality solution for this problem.

Table 1
The number of flux evaluations in each computational step for various schemes, and the computation times with the maximal stable CFL numbers for the smooth problem

Scheme	Nr. of flux evaluations	CFL	CPU time [s]
CF	12	0.85	377
FCF	6	0.57	239
NSS	6	1.0	126
SYS	30	1.0	768
DSBS	21	1.0	894

Table 2
The L_1 density errors for the smooth problem on 50^3 and 100^3 grids along with the order of approximation computed from the ratio of these errors

Scheme	L_1^{50}	L_1^{100}	$\log_2(\frac{L_1^{50}}{L_1^{100}})$
LF	1.78×10^{-1}	9.20×10^{-2}	0.95
CF	1.65×10^{-2}	4.08×10^{-3}	2.02
FCF	1.66×10^{-2}	4.02×10^{-3}	2.05
NSS	1.26×10^{-2}	3.18×10^{-3}	1.99
SYS	1.26×10^{-2}	3.18×10^{-3}	1.99
DSBS	1.26×10^{-2}	3.18×10^{-3}	1.99

5.2.1. Smooth problem

Here we use a problem (generalized to 3D from [5]), with a simple analytic solution, to check the speed, stability, and accuracy of the basic dispersive schemes. The solution is

$$\rho(x, y, z, t) = 1 + \frac{1}{5}\sin\big(\pi\big(x + y + z - t[u + v + w]\big)\big)$$

with constant values of the pressure p and all three velocity components u, v and w. The tests use $p = 0.5$, $u = 0.1$, $v = 0.2$, $w = 0.3$ and a final time $T = 0.5$. The problem is solved in the cube $[0, 2]^3$ using periodic boundary conditions.

In our tests (on 650 MHz Alpha server), we used a grid with 100^3 points. The most time expensive part of a computational step is the evaluation of non-linear fluxes and the number of time steps taken which increases with decreasing maximum stable CFL number. In Table 1 we present CPU time together with number of flux evaluation per time step and the maximum CFL number for all five second-order dispersive schemes.

The fastest scheme is NSS because it uses the smallest number of flux evaluations and it has an optimal stability region. FCF, with the same number of flux evaluations, is slower than NSS by a factor approximately proportional to the ratio of their CFL numbers. CF is slower than NSS and FCF because it uses more flux evaluations. SYS and DSBS are the slowest because of their large number of flux evaluations, with DSBS scheme slower than SYS scheme because of the complexity of formulas (15)–(17) defining the flux.

Table 2 presents L_1 density errors of all schemes, including LF, on 50^3 and 100^3 grids, and the order of approximation computed from the ratio of these errors. As expected, LF is first-order, with all other

Table 3
The L_1 and $L_{\max}$ density errors for each scheme for the Noh problem on 50^3, 100^3 and 200^3 grids

Scheme	L_1^{50}	L_1^{100}	L_1^{200}	$L_{\max}^{50}$	$L_{\max}^{100}$	$L_{\max}^{200}$
LF	3.71	1.88	0.96	40.0	42.1	42.2
CF LF 4	1.62	0.82	0.41	38.2	41.3	40.7
FCF LF 4	2.30	1.11	0.58	37.9	42.1	40.7
NSS LF 4	1.64	0.91	failed	40.3	40.3	failed
SYS LF 4	1.58	0.86	0.45	34.2	36.7	38.1
DSBS LF 4	1.58	0.72	0.40	34.2	41.5	39.9
hybrid DSBS LF	1.22	0.66	0.32	44.7	42.3	45.9

schemes being second-order. NSS, SYS and DSBS have the same accuracy and are more accurate than CF and FCF schemes.

5.2.2. Noh problem

In Fig. 2, we will use five composite schemes to plot the solutions of the classical Noh problem [13], which is a difficult test problem [14]. Because this problem has an analytic solution, we can compute the errors which are given in Table 3. The initial data for the Noh problem are a constant value of pressure ($p = 0$) and density ($\rho = 1$), while the velocity is a unit vector directed towards the origin, and the gas constant is $\gamma = 5/3$. We solve this problem in the unit cube $[0, 1]^3$. The exact solution of this problem is:

$$\rho = \begin{cases} 64 & \text{for } r \leqslant Vt, \\ \left(1 + \frac{t}{r}\right)^2 & \text{for } r > Vt, \end{cases}$$

where $V = 1/3$ is the speed of a moving spherical shock wave, t is the time and r is the distance of a point from the origin. The pressure remains zero outside the spherical shock and is constant inside, $p = 64/3$, while the velocity is zero inside the spherical shock and a unit vector directed towards origin outside. On three faces of the cube going through the origin, the boundary conditions are given by symmetry, while on the other three faces we use exact boundary conditions from the known analytic solution.

Fig. 2 displays the density ρ as a function of r at the time $T = 2.7$, using 90^3 grid points. The exact solution is given by the black line. We can see that for the schemes (c)–(f) derived from the dimensional splitting idea, the density values are more dissipated inside the circular shock than for the schemes (a) and (b). However their dip at the origin is less pronounced. The hybrid DSBSLF scheme (f) has the biggest overshoot on the shock and is more oscillatory as is the case also for the other tests.

The L_1 and $L_{\max}$ errors for the five composite schemes are summarized in Table 3. The LF scheme is the worst because it is only first-order and too diffusive. FCF LF 4 is worse than CF LF 4 probably due to the smaller CFL number causing more time steps. NSS LF 4 failed on the fine grid, probably due to its lack of symmetry. SYS LF 4 is worse than DSBS LF 4 which is slightly better than CF LF 4. From the scatter plots, we know that CF LF 4 has less variation inside the central constant region, however it has bigger dip in the center. The hybrid DSBS LF has the best L_1 errors however the biggest $L_{\max}$ errors as it has the biggest overshoot on the shock and it is oscillatory.

5.2.3. Explosion problem

CF LF 40 is used to simulate an explosion problem inspired by the 2D explosion problem from [17] that generates a spherical wave. By symmetry, we need only solve the problem inside the cube $[0, 1.5]^3$.

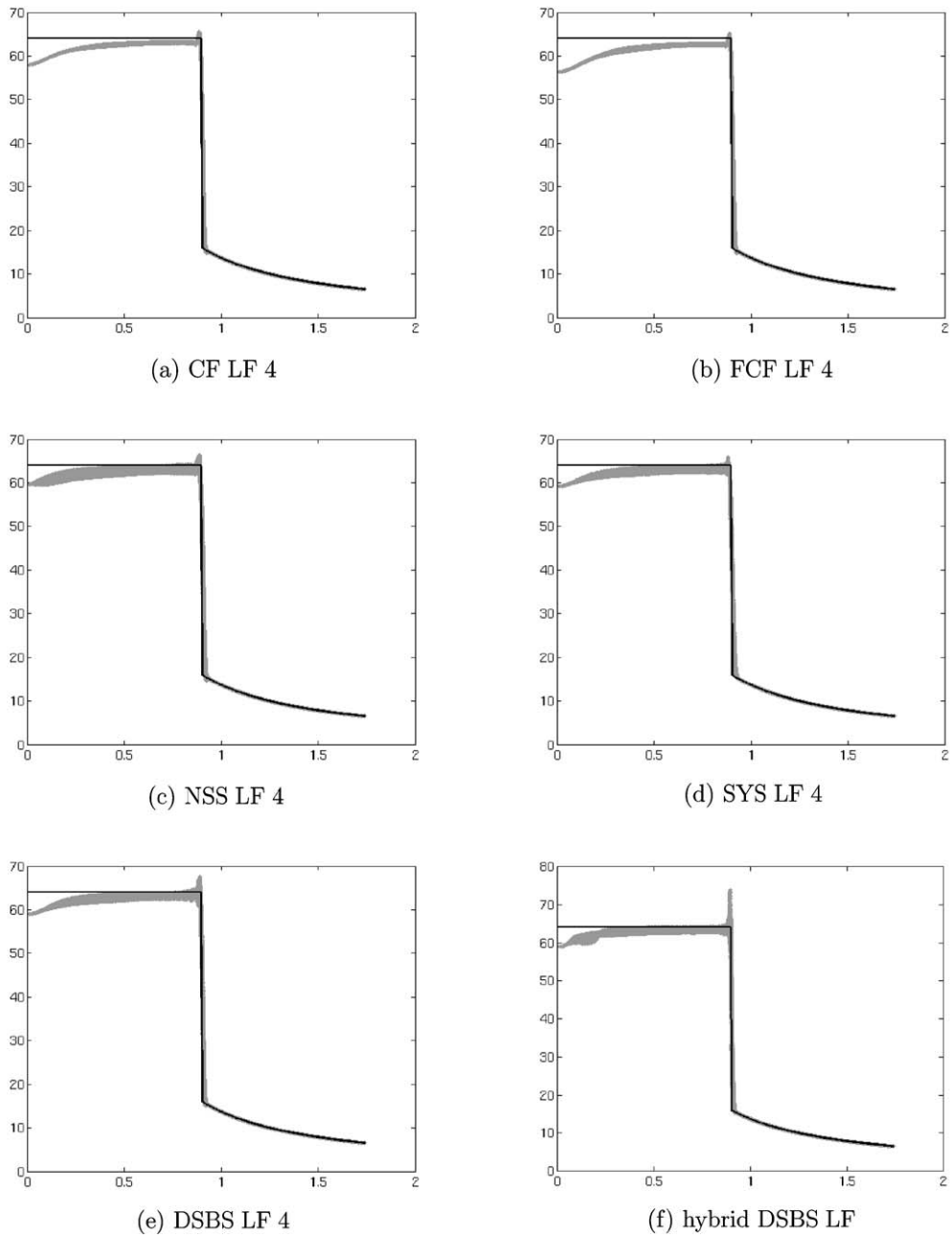

Fig. 2. Scatter plot of the density for the 3D Noh problem computed by (a) CF LF 4, (b) FCF LF 4, (c) NSS LF 4, (d) SYS LF 4, (e) DSBS LF 4 and (f) hybrid DSBS LF using their maximal stable CFL numbers.

The initial velocity is zero while the initial data for the density and pressure have a jump on a sphere of radius 0.4 centered at the origin. Inside the sphere, $\rho = 1$ and $p = 1$, while outside the sphere $\rho = 0.125$ and $p = 0.1$. The gas constant is $\gamma = 1.4$. On three faces of the cube, the boundary conditions are given

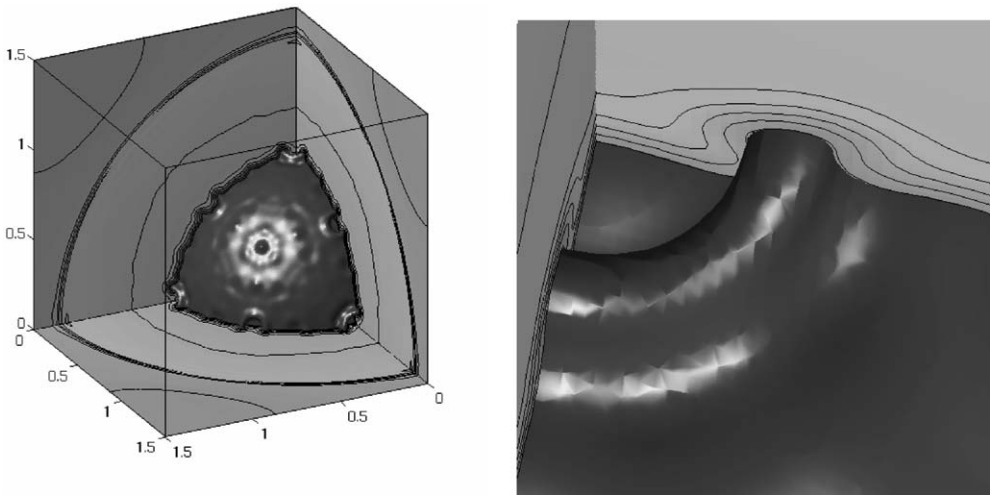

Fig. 3. Density isosurface at the contact wave, combined with three 2D cuts along the coordinate planes, for the solution of the explosion problem computed by CF LF 40 using its maximal stable CFL number. On the right, the upper Rayleigh–Taylor instability is zoomed.

by symmetry, while on the other three faces, free boundary conditions are employed. The solution was simulated to time $T = 2.5$ using a grid with 260^3 points. The use of one diffusive step every 39 dispersive step means that very little diffusion has been added, with more diffusion Rayleigh–Taylor instabilities would not appear.

The solution has a shock that travels away from the center and the contact discontinuity behind the shock. A rarefaction wave goes towards the origin where it is reflected. The contact becomes weaker and after some time it comes to rest and then travels inwards. Rayleigh–Taylor instabilities appear on the surface of the contact wave. Fig. 3 shows the isosurface of density at the contact with three 2D cuts along the coordinate planes at $T = 2.5$.

5.2.4. Riemann problem

The 3D Riemann problem is a generalized version of Riemann problem 4 from [15,9]. The region is the cube $[0, 1]^3$ which is divided in to eight octants that are labeled in the obvious way with the binary numbers 000 through 111, and then using these labels, the initial conditions are presented in Table 4. The value of gas constant is $\gamma = 1.4$. Free boundary conditions are used.

Table 4
Initial values for the Riemann where $\rho_1 = 0.5065$, $\rho_2 = 1.1000$, $p_1 = 0.3500$, $p_2 = 1.1000$ and $v_0 = 0.8939$

Octant	000	100	010	110	001	101	011	111
ρ	ρ_2	ρ_1	ρ_1	ρ_2	ρ_1	ρ_2	ρ_2	ρ_1
u	v_0	0	v_0	0	v_0	0	v_0	0
v	v_0	v_0	0	0	v_0	v_0	0	0
w	v_0	v_0	v_0	v_0	0	0	0	0
p	p_2	p_1	p_1	p_2	p_1	p_2	p_2	p_1

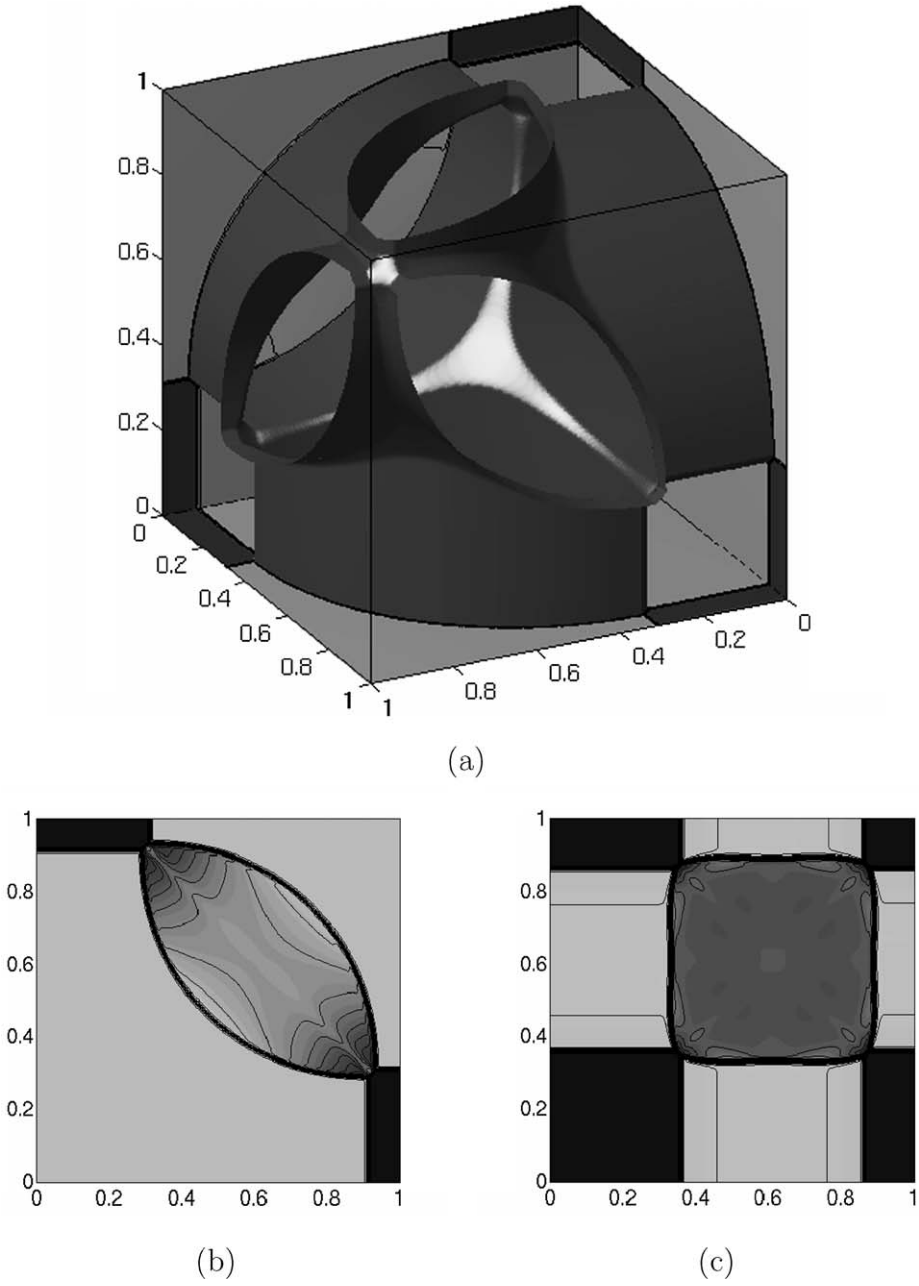

Fig. 4. The solution of the Riemann problem using DSBS LF 4 $T = 0.25$: (a) a global view of the isosurface with density $\rho = 1.5$, (b) the slice in the plane $z = 0$, which should give the 2D solution, (c) the slice in the plane $z = 0.612$, at the middle of the moving 3D object.

We simulate this problem on a very fine grid of size 300^3 using DSBS LF 4 with a CFL number of 1.0 and show the results at time $T = 0.25$ in Fig. 4. Part (b) shows a 2D cut on the face of computational cube that should reproduce the 2D solution and does corresponds well to results from [15,9]. For the 2D

solution, the growing moving lens shaped region between the curved shocks has higher density than the initial density ρ_2, while in 3D there appears a growing moving volume between the surfaces of 3D shock waves with density higher than that in 2D.

6. Conclusion

In 3D, we have created a new Lax–Wendroff-type optimally-stable second-order accurate non-split dispersive scheme that is in conservation form. When combined with the Lax–Friedrichs scheme to make a hybrid scheme, the resulting scheme produces quality simulations of difficult problems.

Acknowledgement

This research was supported in part by the Czech Grant Agency grant 201/00/0586, by the National Science Foundation grant CCR-9531828, by the Ministry of Education of the Czech Republic project MSM 6840770010 and by the US Department of Energy at Los Alamos National Laboratory, under contract W-7405-ENG-36.

References

[1] G.E. Collins, H. Hong, Partial cylindrical algebraic decomposition for quantifier elimination, J. Symbolic Comput. 12 (3) (1991) 299–328.
[2] A. Harten, The artificial compression method for computation of shocks contact discontinuities: III self adjusting hybrid schemes, Math. Comp. 32 (1978) 363–389.
[3] A. Harten, G. Zwas, Self-adjusting hybrid schemes for shock computations, J. Comput. Phys. 6 (1972) 568–583.
[4] H. Hong, R. Liska, S. Steinberg, Testing stability by quantifier elimination, J. Symbolic Comput. 24 (2) (1997) 161–187, Special issue on Applications of Quantifier Elimination.
[5] G.-S. Jiang, C.-W. Shu, Efficient implementation of weighted ENO schemes, J. Comput. Phys. 126 (1996) 202–228.
[6] M. Kuchařik, Diferenční schemata pro zákony zachování ve 3D [Difference Schemes for Conservation Laws in 3D], Master's thesis, Czech Technical University, 2002.
[7] C.B. Laney, Computational Gasdynamics, Cambridge University Press, Cambridge, 1998.
[8] J.O. Langseth, R.J. LeVeque, A wave propagation method for three-dimensional hyperbolic conservation laws, J. Comput. Phys. 165 (2000) 126–166.
[9] P.D. Lax, X.-D. Liu, Solution of two dimensional Riemann problem of gas dynamics by positive schemes, SIAM J. Sci. Comput. 19 (2) (1998) 319–340.
[10] R.J. LeVeque, Numerical Methods for Conservation Laws, Birkhäuser, Basel, 1990.
[11] R. Liska, B. Wendroff, Composite schemes for conservation laws, SIAM J. Numer. Anal. 35 (6) (1998) 2250–2271.
[12] R. Liska, B. Wendroff, Composite centered schemes for multidimensional conservation laws, in: M. Fey, R. Jeltsch (Eds.), Hyperbolic Problems: Theory, Numerics, Applications, Seventh International Conference in Zürich, February 1998, vol. II, Internat. Ser. Numer. Math., vol. 130, Birkhäuser, Basel, 1999, pp. 661–670.
[13] W.F. Noh, Errors for calculations of strong shocks using an artificial viscosity and artificial heat flux, J. Comput. Phys. 72 (1987) 78–120.
[14] W.J. Rider, Revisiting wall heating, J. Comput. Phys. 162 (2000) 395–410.
[15] C.W. Schulz-Rinne, J.P. Collins, H.M. Glaz, Numerical solution of the Riemann problem for two-dimensional gas dynamics, SIAM J. Sci. Comput. 14 (1993) 1394–1414.
[16] G. Strang, On the construction and comparison of difference schemes, SIAM J. Numer. Anal. 5 (3) (1968) 506–517.
[17] E.F. Toro, Riemann Solvers and Numerical Methods for Fluid Dynamics, Springer, Berlin, 1997.